Optical properties of CdSe/MgS monolayer quantum wells and self-assembled quantum dots

M. Funato,* K. Omae,[†] Y. Kawakami, and Sg. Fujita
Department of Electronic Science and Engineering, Kyoto University, Kyoto, 615-8510, Japan

C. Bradford, A. Balocchi, K. A. Prior, and B. C. Cavenett
Department of Physics, Heriot-Watt University, Edinburgh, EH14 4AS, United Kingdom
(Received 30 March 2006; published 8 June 2006)

The optical properties of CdSe/MgS monolayer (ML) quantum wells (QW's) and self-assembled quantum dots (QD's) grown by molecular beam epitaxy are investigated by continuous-wave (cw) and time-resolved (TR) photoluminescence (PL) spectroscopy. The cw-PL spectra clearly show the growth development from ML-QW to QD's as the CdSe thickness increases from 1 to beyond 3 ML. The carrier dynamics are characterized chiefly by TRPL. For ML-QW's, it is determined that carrier localization in the potential fluctuations and scattering by phonons significantly influence the optical properties. On the other hand, TRPL reveals the carrier dynamics for QD's and a wetting layer (WL); some of the carriers photogenerated in the WL radiatively emit, while others are captured by QD's via a carrier-carrier scattering on a ~5 ps time scale. Within the next 10–50 ps, the carriers relax to the ground level via a carrier–LO–phonon scattering. Finally, the carriers radiatively recombine with a recombination lifetime of 100–300 ps, depending on the emission energy.

I. INTRODUCTION

Carrier confinement in quasi-zero-dimensional semiconductor systems has attracted intensive research from both pure and applied points of views.[1] Perhaps the most thoroughly studied systems involve InAs self-assembled quantum dots (QD's) on GaAs substrates. On the other hand, there is considerable interest in wide-band-gap II-VI QD's for visible emitters and spintronic applications.[2–4] Since CdSe on ZnSe and InAs on GaAs have nearly identical lattice mismatches, their growth behaviors had been expected to be similar. Actually, the formation of self-assembled CdSe QD's on ZnSe was initially explored by Xin *et al.*,[5] and numerous others have followed.[6–8] Compared to InAs/GaAs, CdSe/ZnSe has a stronger confinement of carriers and stronger excitonic properties, which allow highly efficient luminescence at elevated temperatures. In fact, a single-photon emitter based on CdSe/ZnSe QD's can operate up to 200 K.[9] However, to enhance the excitonic properties and to achieve a higher luminescence efficiency particularly at room temperature (RT), further confinement is necessary. Furthermore, the CdSe/ZnSe interface is highly miscible, and consequently, the interfaces become unclear,[8,10] which makes for a gradual carrier confinement. Thus, the exact size and composition of the dots are unknown. In order to overcome these issues, we proposed that MgS is a promising alternative to ZnSe.

Zinc-blende (ZB) MgS has a band gap of ~4.8 eV and a lattice parameter close to GaAs and ZnSe.[6,11] Hence, ZB-MgS is an excellent barrier material for wide-gap II-VI quantum structures. Although the stable MgS crystal structure is rocksalt, we recently established a molecular beam epitaxy (MBE) technique that enables ZB-MgS to be grown on lattice-matched GaAs substrates.[11] Thus, it is possible to fabricate MgS-based quantum structures on GaAs. A detailed study of the excitonic properties of high-quality ZnSe/MgS quantum wells (QW's) has already been reported.[11] Also, we have observed the details for the formation of ML-QW's and

QD's while growing CdSe on MgS using optical spectroscopy.[12] Since the strain in the CdSe/MgS system is nearly identical to that in CdSe/ZnSe, the growth behavior of CdSe on MgS should be similar to that on ZnSe. However, dot formation in CdSe/MgS is clearly different from CdSe/ZnSe. For example, during the growth of the CdSe QD's on ZnSe, there is intermixing between the CdSe and ZnSe layers so that CdZnSe dots are formed. There is little evidence of a wetting layer (WL), and not only Stranski-Krastanow (SK) dots, but also dotlike islands grow with a density of ~10^{10} cm^{-2} and 10^{11} cm^{-2}, respectively.[13] In contrast, optical spectroscopy of CdSe/MgS provides clear evidence of monolayer (ML) QW's and WL formation, which indicates that when growing CdSe/MgS dots intermixing does not occur. In order to assess the miscibility of the MgCdSSe alloy, the spinodal curve was calculated similar to that for of MgZnSSe (Ref. 14) and the result is shown in Fig. 1. The temperature of 240 °C assumed in this calculation is a typical growth temperature in this study. It is clear that the MgCdSSe system is immiscible throughout the entire composition, which is consistent with our experimental results.

The CdSe/MgS system is also important due to the much stronger exciton confinement. Based on the linear combination of atomic orbitals (LCAO) theory,[15] the evaluated conduction- and valence-band offsets at the CdSe/MgS interface are 2.16 and 0.87 eV, respectively, which are much larger than those in the CdSe/ZnSe system (0.84 and 0.23 eV). Using these band offsets, we calculated the exciton binding energies for CdSe/MgS QW's as well as CdSe/ZnSe QW's for comparison. The CdSe well involves compressive strain, and so heavy-hole exciton was considered. The calculation was performed by adopting Peyla's method.[16] Figure 2 shows the results when the longitudinal axis shows the difference between the 1*s* and 2*s* heavy-hole exciton binding energies. It is determined from Fig. 2 that the decrease in the binding energy due to tunneling effects observed in CdSe/ZnSe QW's that are narrower than 3 ML does not occur even in 1-ML CdSe/MgS QW's (1 ML
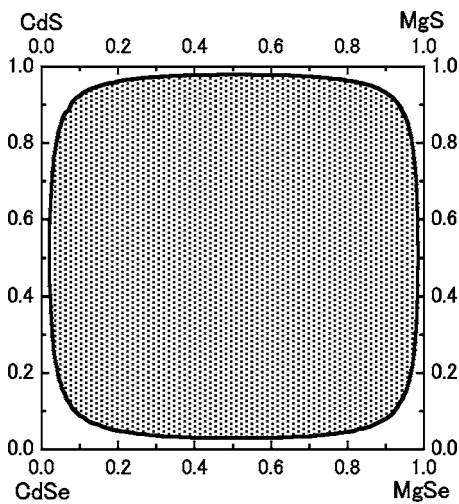
FIG. 1. Spinodal curve for MgCdSSe alloy at a typical growth temperature of 240 °C. The shaded region indicates the immiscible region.

FIG. 2. Heavy-hole exciton binding energy for CdSe/MgS and CdSe/ZnSe QW's.

=0.33 nm, when CdSe is coherently grown). Obviously, MgS is advantageous over ZnSe in terms of exciton stability.

Finally, it is noteworthy that the fluctuations of the well width, and consequently the transition energy, are in actual QW's and are responsible for the deviation from the ideal two-dimensional character. The interface fluctuations, particularly in narrow QW's, produce potential minima—that is, localization states for the excitons. It has been previously reported that these localization states act as QD's (Ref. 17) and give rise to the existence of zero-dimensional excitons. Since the confinement potential in the CdSe/MgS system is very large, the interface fluctuations should provide significantly deep localization states in the CdSe/MgS ML-QW's. Thus, the localized quasi-zero-dimensional excitons should play a key role in determining the optical properties in both CdSe/MgS QD's and CdSe/MgS ML-QW's.

In this paper, we review the growth and optical properties of recently developed CdSe/MgS ML-QW's and QD's. We also present a detailed study of the recombination processes using picosecond time-resolved (TR) photoluminescence (PL) spectroscopy. The paper is organized as follows. Section II theoretically predicts the excitonic properties of
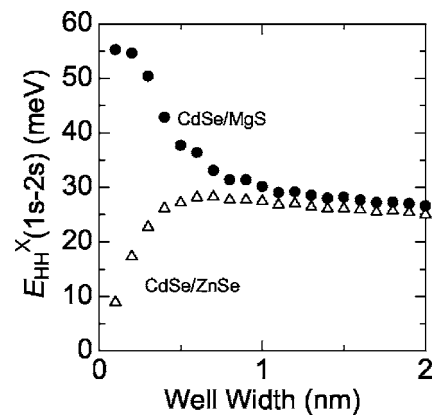
CdSe/MgS quantum disks. After a brief description of the experimental method in Sec. III, the growth development from ML-QW's to QD's is described in Sec. IV. Then the carrier dynamics in ML-QW's and QD's are investigated in Secs. V and VI, respectively.

II. THEORETICAL PREDICTIONS

The excitonic properties such as transition energy, binding energy, and spontaneous-emission lifetime are theoretically predicted for the CdSe/MgS system. Since CdSe is compressively strained, $1s$ heavy-hole excitons are considered. As mentioned in the Introduction, zero-dimensional excitons would govern the optical properties of CdSe/MgS ML-QW's and QD's; a quantum disk structure was assumed for this calculation. The calculation was based on Ref. 18, where the disk possesses a cylindrical shape, and the vertical and lateral confinements are described by a rectangle potential like in normal QW's and harmonic-oscillator-type parabolic potentials, respectively. The only difference from Ref. 18 is the transition matrix element for bulk materials, and we used the one proposed by Yan *et al.*[19] The temperature was assumed to be 0 K, and so no thermalization was considered.

The results are shown in Fig. 3, and the parameters used are listed in Table I. Figure 3(a) indicates that the CdSe/MgS
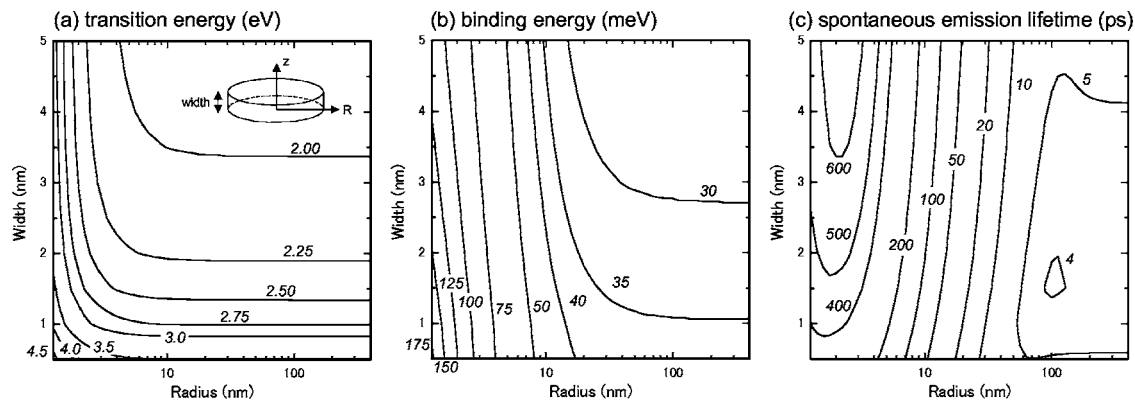

FIG. 3. Contour plots of transition energy, binding energy, and spontaneous emission lifetime of $1s$ heavy-hole excitons in CdSe/MgS quantum disks.

TABLE I. Physical parameters used for the calculation.

	MgS	CdSe
Energy gap (eV)	4.8	1.766[a]
Valence band offset (eV)		0.87[b]
SO splitting energy (eV)	0.07[c]	0.42[a]
Effective masses ($/m_0$)		
Electron	0.25[d]	0.13[e]
Heavy hole ∥ [001]	1.4[d]	0.45[e]
Heavy hole ⊥ [001]	0.41[d]	0.158[f]
Lattice parameter (nm)	0.562[g]	0.6077[h]
Static dielectric constant	7[i]	9.2[j]
Deformation potentials (eV)		
Hydrostatic	−5.56[d]	−3.66[e]
Shear	−1.35[d]	−0.8[e]
Elastic stiffness constant ($\times 10^{10}$ N/m^2)		
C_{11}	5.68[d]	6.67[e]
C_{12}	5.79[d]	4.63[e]

[a]Reference 20.
[b]Estimated by the LCAO theory. See the text for more details.
[c]The value for ZnS was used for MgS as these materials possess a common anion (S) and, consequently, are expected to have similar valence band electronic structures.
[d]Reference 21.
[e]Reference 22.
[f]Reference 23.
[g]Reference 24.
[h]Reference 25.
[i]Roughly estimated from other II-VI's such as ZnX, CdX, and HgX (X=S, Se, Te).
[j]Determined to give the bulk exciton binding energy of 16 meV.

QD's can cover almost the entire visible spectral range. From Fig. 3(b), on the other hand, it is found that the exciton binding energy can be larger than the thermal energy of RT (26 meV) and, also, the CdSe LO phonon energy (26 meV) for any disk dimensions. Therefore, excitons in CdSe disks embedded in MgS will be stable even at RT. Furthermore, Fig. 3(c) shows that the radiative lifetime is more than 2 times shorter, compared with conventional InAs QD's. This is mostly due to the wider band gap, which enlarges the oscillator strength. A shorter radiative lifetime brings a better internal quantum efficiency, and, therefore, the predicted short spontaneous-emission lifetime and the large binding energy in the CdSe/MgS QD's are expected to lead to highly efficient excitonic devices operating at elevated temperatures.

III. EXPERIMENT

The samples were grown on GaAs(001) substrates by MBE and have the structure GaAs (substrate)/ZnSe (50 nm, buffer)/MgS (20 nm)/CdSe/MgS (10–20 nm)/Zn(Mg)(S)Se (5 nm, protective cap). The detailed growth method for MgS has been described previously.[11] CdSe layers were deposited at 240 °C using either MBE or migration
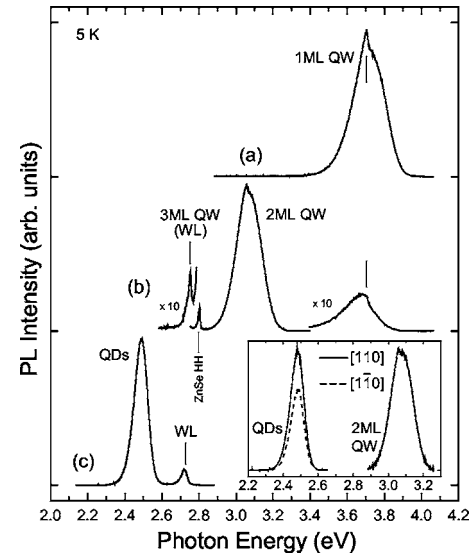

FIG. 4. Low-temperature (5 K) PL spectra of ML-QW's [(a) and (b)] and (c) QD's. The nominal CdSe thicknesses are (a) 1 ML, (b) 2 ML, and (c) >3 ML. The ZnSe heavy-hole (HH) emission is from the buffer layer. The inset shows the polarization PL spectra for 2 ML QW and QD's acquired along the [110] and [1$\bar{1}$0] directions.

enhanced epitaxy (MEE). However, there was no discernible difference in the PL properties due to the growth methods. CdSe layers grown by MBE were deposited with a low growth rate of 50 nm/h, and subsequently annealed at 280 °C for approximately 5 min,[26] though, in fact, no noticeable difference was observed in the optical properties with and without annealing. The MEE layers were also annealed at 280 °C. Layer morphology was monitored during growth using reflection high-energy electron diffraction (RHEED) while the sample structural quality of the CdSe layers was obtained after growth using x-ray double-crystal diffraction.

For cw-PL, an Ar$^+$ laser with a wavelength from 285 to 514 nm was used for an excitation. PL excitation (PLE) spectra were obtained by scanning the wavelength from a cw-dye laser excited by the Ar$^+$ laser. TRPL measurements were performed at 13 K unless stated, using 1.5-ps excitation pulses at a repetition rate of 80 MHz from a frequency-doubled Ti-sapphire laser and detection was via a 25-cm monochromator and a streak camera. The laser was tuned to a wavelength of 356 nm (3.48 eV) for the ML-QW's and 400 nm (3.10 eV) for QD's in order to selectively excite CdSe.

IV. GROWTH DEVELOPMENT FROM ML-QW TO QD's

The growth development from ML-QW to QD's was assessed by PL and atomic force microscopy (AFM). Figure 4 shows the low-temperature (5 K) PL spectra of ML-QW's [(a) and (b)] and (c) QD's. The nominal CdSe thicknesses are (a) 1 ML, (b) 2 ML, and (c) >3 ML, and the assignment of the emissions is described in Ref. 12. For the 1-ML and 2-ML emissions, a sharp emission due to CdSe regions 1 or
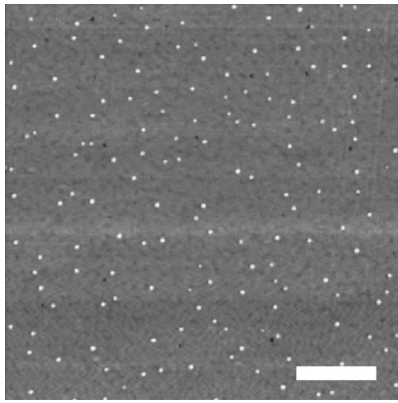
FIG. 5. Typical AFM image of QD samples without MgS caps. The marker represents 1 μm.

2 ML high which are large in terms of the exciton Bohr radius (4.8 nm for bulk CdSe) overlaps a broad emission, about 200 meV wide, corresponding to the changes in emission energy for size fluctuations away from perfect ML-QW's. The broad emissions from the ML-QW's characterize the CdSe/MgS system because, for the CdSe/ZnSe system, a narrower ML-QW exhibits a narrower emission[10,27] due to interfacial alloy formation.[10] Clearly in the present case there is no significant interdiffusion between Mg and Cd, consistent with Fig. 1. Increasing the CdSe thickness beyond 3 ML causes the appearance of an emission with a broad linewidth due to QD formation by SK growth and a WL emission corresponding to the 3 ML QW energy [Fig. 4(c)]. The QD formation was demonstrated by polarization PL measurements along the [110] and [1$\bar{1}$0] directions, as shown in the inset. For the 2-ML QW, the PL spectra acquired along both the directions are identical, while for the QD's, the PL spectrum along the [110] direction is stronger by ~45%, which indicates that the shape of the emission sites is isotropic in the ML-QW and is deformed to be anisotropic by the QD formation. The general relationship between the emission intensity and wave vector suggests that the observed 45% increase in the emission intensity corresponds to the elongation of the QD shape along the [110] direction by about 20%.

QD samples have been grown without MgS caps for AFM measurements. The presence of QD's is observed only on layers with more than 3 ML deposited, and a typical image from such a layer is shown in Fig. 5. The dots are approximately 16 nm high and 60 nm in diameter, and the dot density is 5×10^8 cm^{-2}. The section analysis indicated an almost atomically flat surface between the dots, which corresponds to the narrow 3-ML (WL) emission peak observed in Fig. 4. An anisotropic shape predicted by the above PL measurements was not detected within the present experimental resolution.

V. MONOLAYER QUANTUM WELLS

A. cw-PL

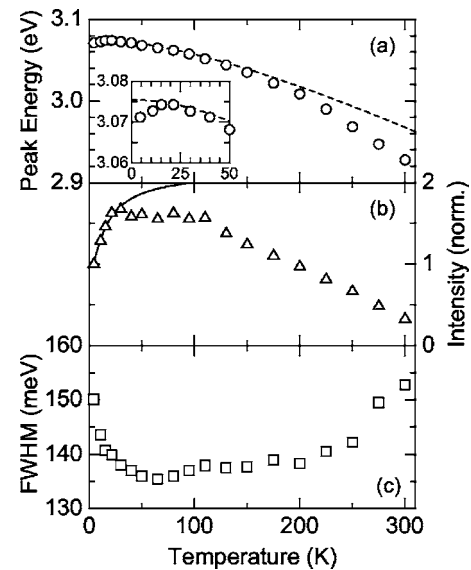The temperature dependences of the cw-PL were investigated by exciting the CdSe/MgS ML-QW's with the 351-

FIG. 6. Temperature dependence of (a) the PL peak energy, (b) the integrated intensity, and (c) the linewidth of the 2-ML QW emission. In (a), the dashed line is the band gap of CdSe (Ref. 20) shifted to a higher energy for comparison with the data, and the inset shows a detailed variation of the PL peak energy below 50 K. The solid line in (b) is a fit to the data as described in the text (reproduced from Ref. 12).

nm line (3.53 eV) of the Ar$^+$ laser to ensure not to excite the MgS barrier layer. Typical results are summarized in Fig. 6 for the 2-ML QW emission. First, it should be emphasized that the integrated intensity at RT is still ~33% of the intensity at 5 K, indicating a high internal quantum efficiency probably due to the strong confinement, as discussed with Fig. 2 and in Sec. II. When the temperature is increased up to 50 K, the emission energy is blueshifted [inset of Fig. 6(a)]. Also, the integrated intensity increases and the full width at half maximum (FWHM) decreases. With a further increase in temperature above 50 K, the emission energy is redshifted, the integrated intensity decreases, and the FWHM increases. These quite anomalous temperature dependences are understandable in terms of excitons localized by potential fluctuations as illustrated schematically in Fig. 7(a). Further evidence of the presence of localized excitons is given later by TRPL. An example that can realize such potential fluc-
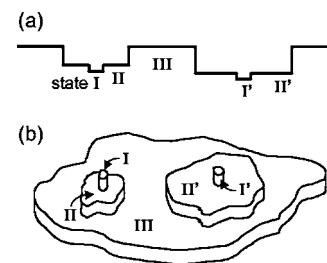

FIG. 7. (a) Schematic of potential fluctuations used for the explanation of the PL temperature dependence shown in Fig. 6. (b) An example of the layer growth that could realize the potential fluctuations in (a), where I and II are CdSe islands and III is either a CdSe ML or the MgS barrier layer. (Reprinted from Ref. 12).

tuations is CdSe ML islands with size fluctuations as shown in Fig. 7(b), where sets of type-I and -II islands grow on either an extended CdSe ML or the MgS barrier layer (III).

The temperature dependence below 50 K is explained well by exciton repopulation from localized states I to relatively free states II. Since such repopulation weakens the exciton localization, the spontaneous-emission lifetime becomes shorter [cf. Fig. 3(c)], and as a consequence, the PL intensity can be stronger. We have performed a model calculation, assuming that some excitons in the lower-energy state (state I) are thermally repopulated into the higher-energy state (state II) with a Boltzmann distribution.[12] The result is shown by the solid line in Fig. 6(b). Very good agreement was found with an energy difference between two levels of 1.3 meV, which agrees reasonably well with the amount of blueshift of about 4 meV estimated from the inset of Fig. 6(a). Furthermore, the decrease of the FWHM supports this model because the repopulation reduces the number of the sites contributing to the emission, resulting in the reduction of the emission energy distribution.

Between 50 K and 120 K, the emission energy simply follows the temperature dependence of the CdSe band gap, indicating that the transfer from state I to II is completed in this temperature range and that the emission from state II determines the PL properties.

For the temperature range above 120 K, the exciton transfer between the type-II CdSe islands via state III should be considered; excitons photogenerated homogeneously can escape from a higher-energy II state (e.g., smaller CdSe island) and are retrapped in a lower-energy II′ state (larger CdSe island). Among several possible causes of the carrier escape, phonon scattering is plausible in our ML-QW's as discussed in Sec. V B. This exciton transfer process involves a redshift of the emission energy, consistent with the experimental results. Also, the FWHM narrowing between 150 and 200 K is consistent with this transfer model. The decrease of the integrated intensity is due to nonradiative recombination, as is discussed in Sec. V B.

B. Carrier dynamics

The carrier dynamics in a CdSe/MgS QW with a well about 2 ML thick have been characterized. The excitation power was 2.5 μJ/cm^2 unless otherwise stated.

1. Carrier dynamics at low temperatures

The time-integrated PL spectrum of the CdSe/MgS ML-QW taken at 13 K is shown in Fig. 8(a). The PL decay at the peak was shown in Fig. 8(b). As can be seen, the PL decay has two components and so the curve was fitted by

$$I = I_{\text{offset}} + A_{\text{fast}} \exp\left(-\frac{t}{\tau_{\text{fast}}}\right) + A_{\text{slow}} \exp\left(-\frac{t}{\tau_{\text{slow}}}\right). \quad (1)$$

Let us consider the origins of these two decay components. The inset of Fig. 8(b) is the variation of the intensities of A_{fast} and A_{slow} as a function of the excitation power. As seen, A_{fast} is always dominant and almost proportional to the excitation power, while A_{slow} saturates at above 3×10^{-1} μJ/cm^2, sug-
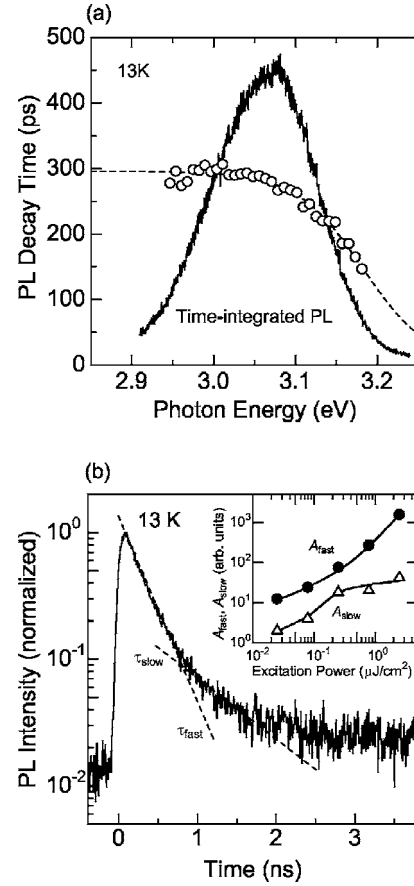

FIG. 8. (a) Time-integrated PL spectrum and PL decay time (τ_{fast}) of the CdSe/MgS ML-QW. The dashed line is the result of a fit; see the text for details. (b) PL decay curve at the emission peak. The inset illustrates the variation of the fast- and slow-decay components as a function of the excitation power, which was extracted by the fit using Eq. (1).

gesting that the fast decay is related to radiative recombination and that the slow decay is related to states with a low density of states. We discuss the nature of the slow decay later in Sec. V B 2 and here would like to concentrate on the fast decay.

The dependence of the PL fast decay on the emission energy was plotted in Fig. 8(a). The lifetime is shorter for higher emission energy. This behavior is explained well by considering carrier transport from higher-energy states to lower-energy localized states. According to the weakly localized model proposed first for CdSSe alloys by Gourdon and Lavallard,[28] the PL decay time τ_{PL} for excitons in localized states can be written as

$$\tau_{\text{PL}}(E) = \frac{\tau_{\text{r}}}{1 + \exp\{(E - E_{\text{me}})/E_0\}}, \quad (2)$$

where τ_{r} is the radiative lifetime, E_{me} is the energy for which the radiative lifetime equals the transfer lifetime, E_0 is a characteristic energy for the localized tail states, and the density of states is assumed to be proportional to $\exp(-E/E_0)$. Above E_{me}, excitons transfer toward lower-energy states rather than recombine radiatively. The dashed line in Fig.
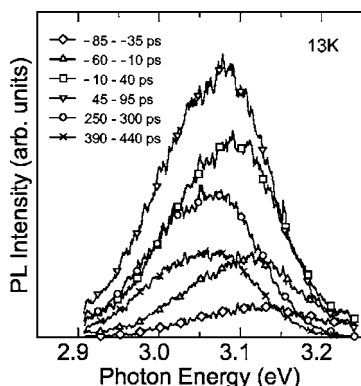
FIG. 9. TRPL spectra. The origin of time is when the laser intensity for excitation reaches the maximum.

8(a) is the best fit between experiments and Eq. (2). The obtained quantities were $\tau_r = 296$ ps, $E_{me} = 3.1824$ eV, and $E_0 = 40.7$ meV. The very good agreement supports that the fast decay observed in Fig. 8(b) is determined by the competition between radiative recombination and exciton transfer.

In cw-PL at low temperatures, the emission from states I and II determines the PL properties as discussed with Figs. 6 and 7 while in TRPL the fast decay is dominant at 13 K. This strongly suggests that the fast decay is related to states I and II and that these states are weakly localized states. The energy dependence of the fast decay observed in Fig. 8(a) is, then, interpreted as the carrier transfer from states I and II with a higher energy to other states I and II with a lower energy.

Evidence of the exciton transfer is also given by TRPL spectra shown in Fig. 9. At first (see ◇ and △), the PL comes from the higher-energy side of the time-integrated PL spectrum [Fig. 8(a)]. Then, the PL peak shifts toward lower energy. At the time of 45–95 ps, the PL intensity is strongest with a peak at 3.08 eV and the spectrum is almost identical to the time-integrated PL spectrum. These results indicate that excitons are first captured by higher-energy states and then travel toward lower-energy states. A further increase in time brings a further redshift and a decrease in the PL intensity, reflecting the faster PL decay for higher energy, as shown in Fig. 8(a).

2. Temperature dependences

Figure 10 shows the temperature dependence of the PL decay measured at the peak. At 13 K, the PL decay is dominated by the fast decay with a lifetime of 280 ps and the slow decay (2.6 ns) is not significant, as already discussed with Fig. 8. At elevated temperatures, the fast-decay component becomes weaker and disappears at around 175 K. Above 175 K, an additional slower decay (1.6 ns at 225 K) appears. These characteristics are quantitatively plotted in Fig. 11, in which the transitions are named as *A*, *B*, and *C*.

Transition *A* is dominant below 150 K. Its lifetime, which is almost equal to the radiative lifetime as shown in Fig. 8(a), decreases with increasing temperature up to 60 K and stays constant at 210 ps at between 60 and 135 K. It is interesting
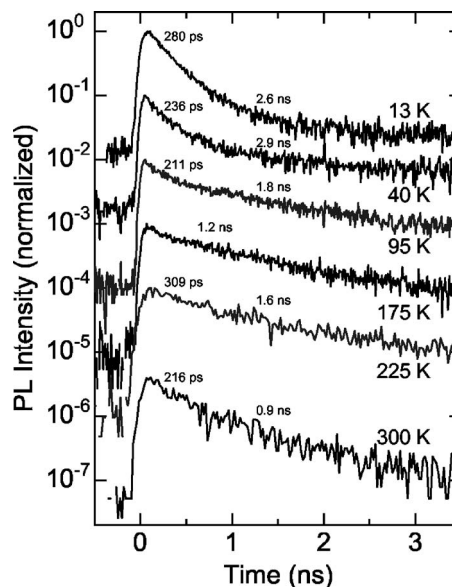

FIG. 10. Decay curves of the PL peak at various temperatures.

to compare this behavior with the temperature dependence of the cw-PL intensity [Fig. 6(b)]; the degree of the lifetime decrease (67%) corresponds well with that of the intensity increase [150% = 1/(67%)]. With Figs. 6 and 7, we proposed a model in which the PL intensity is strengthened by a decrease of the radiative lifetime due to the exciton thermalization. Figure 11 supports this model and confirms that transition *A* involves the radiative recombination from states I and II. The small difference in the lifetime does not allow their recombination lifetimes to be resolved in the decay curves.

Transition *B*, on the other hand, becomes dominant above ~150 K. Note that a redshift of the peak position occurs in this temperature range, as shown in Fig. 6(a). These results suggest that transition *B* is related to localized states deeper than states I and II, the density of which is not so high, as concluded with the inset of Fig. 8(b). Therefore, transition *B* should have a longer radiative lifetime than transition *A*, which is confirmed below. The PL decay time for transition
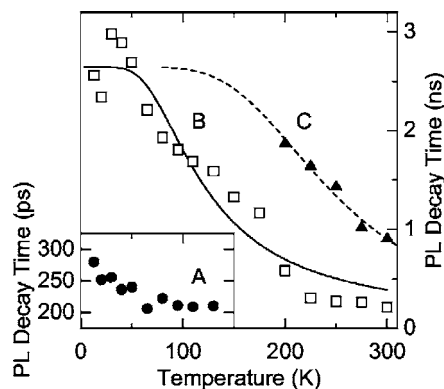

FIG. 11. Temperature dependence of the PL decay times. The solid and dashed lines are the results of fitting assuming an exciton-phonon interaction.

B gradually decreases with temperature. We fitted the experimental result using $\tau_{PL}^{-1} = \tau_r^{-1} + \tau_i^{-1}$, where τ_i represents processes other than the radiative one—that is, for example, nonradiative recombination and carrier transfer. An issue in the fit is how to express the temperature dependences of τ_r and τ_i. The radiative lifetime τ_r is assumed to be temperature independent as excitons associated with transition *B* are deeply localized and the lifetime of localized excitons should be temperature independent.[18] For other processes, there are several possible routes such as defects, exciton thermalization, or exciton-phonon scattering. However, if the lifetime of the defect-related nonradiative recombination (τ_{nr}) is written as $\tau_{nr} \propto T^{-1}$ (Ref. 29) or $\tau_{nr} \propto T^{-1/2}$ (Ref. 49), the experimental results are not reproduced at all. Also, the exciton thermalization may be ruled out as the lifetime for transition *B* begins to decrease at a very low temperature, which does not fit the fact that the exciton confinement in the present sample is very strong. Therefore, phonon processes were considered. Since phonons obey the Bose-Einstein distribution, the lifetime of the phonon process τ_{PH} can be expressed as

$$\tau_{PH}^{-1} = \Gamma_0 \prod_{i=1}^{m} \left[\frac{1}{\exp(E_{PHi}/kT) - 1} + A_i \right]^{n_i}, \qquad (3)$$

where Γ_0 is a constant containing the usual scattering matrix elements, *m* is the number of the type of phonons, E_{PH} is the phonon energy, *A* equals 0 for phonon absorption or 1 for emission, and *n* is the number of phonons.[30] In order to simplify the fitting, we will neglect the contribution from LA phonons in the following discussions, as the LA phonon energy is very small. In the present case, since we are considering the phonon scattering as the nonradiative process, LO phonons are absorbed ($A=0$) and $\tau_i = \tau_{PH}$. The solid line drawn in Fig. 11 is the best fit, and $\tau_r = 2.64$ ns, $m=1$, $E_{PH} = 27.7$ meV, and $n=1$ were obtained. Note that E_{PH} (27.7 meV) is nearly equal to the CdSe LO phonon energy (26 meV) and, furthermore, that a redshift was observed in cw-PL [Fig. 6(a)]. These findings suggest that, above 150 K, an exciton is scattered from state II by one CdSe LO phonon and then recaptured by deeper states.

Transition *C* was not dominant at any temperature. At present, we consider that this transition has an origin similar to transition *B* but involves multiphonon processes. This is because a fit using the same τ_r and E_{PH} as those in the above calculation brought $n=2.2$, and the fit is fairly good as shown by the dashed line in Fig. 11. Namely, transition *C* is related to deeper states and an exciton scattered by two CdSe LO phonons is responsible to transition *C*.

It is interesting to note that transitions *B* and *C* suggest the presence of levels about 30–60 meV deep and that these levels can be responsible for the redshift of about 30 meV observed in cw-PL.

VI. QUANTUM DOTS

A. cw-PL

PL measurements of the QD samples were performed under the same experimental conditions as the ML-QW PL.
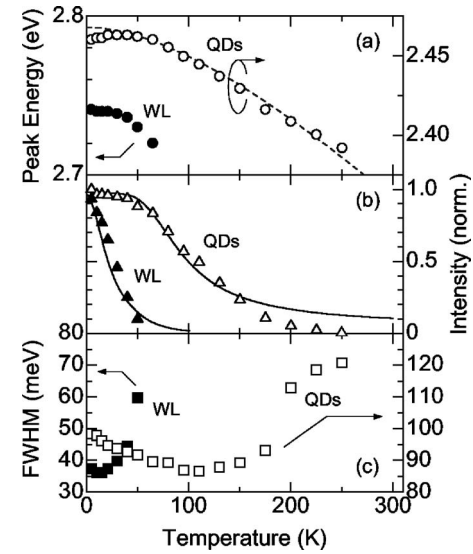

FIG. 12. Summary of the temperature dependence measurement for the QD sample with the PL spectrum at 5 K shown in Fig. 4(c). The dashed line in (a) is the shifted band gap of CdSe. The solid lines in (b) are the result of the simulations based on the rate equations. (Reproduced from Ref. 12).

The temperature dependences of the PL from the QD's and WL are shown in Fig. 12. To explain the temperature dependence of the intensity, we solved rate equations which take the transfer between QD's and WL into account.[12] The results of fitting the data are shown by the solid lines in Fig. 12(b). Fairly good agreement demonstrates the presence of the carrier transfer between QD's and WL described well by the rate equations. The carrier transfer is also discussed in the following Sec. VI B. From the calculation it was found that the parameter which dominates the thermal quenching of the QD PL is the energy for the thermal activation of carriers, which was evaluated to be 28 meV. The origin of this activation energy is uncertain but it is consistent with a phonon process since the CdSe LO phonon energy is 26 meV.

The low QD density estimated by AFM (Fig. 5) suggests the absence of exciton transfer between QD's in the present sample. Therefore, the blueshift observed for the QD emission below 50 K, which cannot be described by the above rate equations, is possibly due to the exciton transfer within each QD with relatively large dimensions. The narrowing of the linewidth in this temperature range supports this hypothesis because such a transfer can reduce the number of emission sites. Above 50 K, the peak energy almost follows the temperature dependence of the bulk CdSe band gap, indicating the absence of any exciton transfers, which would give a redshift. For the WL, the data above 50 K are less reliable as the weak WL emission is on the tail of the strong QD emission. The slight redshift observed for the WL in Fig. 12(a) is due to this uncertainty and the peak energies should follow the CdSe bulk band gap.

It is interesting to compare the temperature dependence of the FWHM in the CdSe/MgS QD's with that in CdSe/ZnSe QD's.[31] The tendencies characterized by the U shape are quite similar to each other. However, the FWHM for the CdSe/ZnSe QD's doubles at a temperature near 280 K,
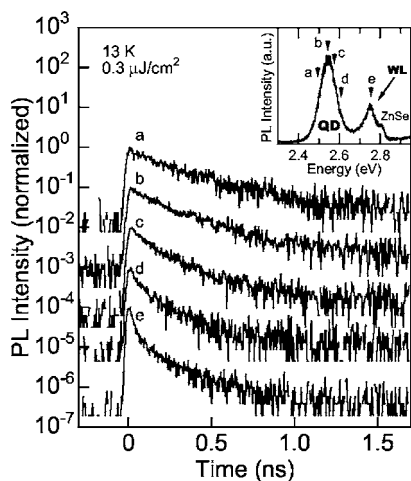
FIG. 13. PL decays taken at the energy positions designated by arrowheads in the inset, where the time-integrated PL spectrum is shown. The excitation power was 0.3 μJ/cm^2.

which makes a striking contrast with the FWHM for the CdSe/MgS QD's broadened by only 30%. This is probably due to the strong confinement in the CdSe/MgS QD's that can prevent carrier–LO-phonon scattering. The thermal quenching of the PL intensity caused by scattering with LO phonons should also be suppressed in the CdSe/MgS QD's, which may improve the internal efficiency.

B. Carrier dynamics

The excitation power was varied between 0.03 and 3 μJ/cm^2. Since the excitation energy was 3.10 eV, CdSe was excited selectively. Assuming the CdSe thickness of 3 ML (=1 nm) is equal to the WL thickness and a CdSe absorption coefficient of 2×10^5 cm^{-1},[32] it is found that only 2% of the excitation power is used to generate carriers in CdSe. The AFM image in Fig. 5 indicated a typical QD density of 5×10^8 cm^{-2}, and, therefore, under an assumption that all photogenerated carriers are finally captured by the QD's, the number of excitons in each QD per pulse is evaluated to be at the most 200 for 3 μJ/cm^2 and 2 for 0.03 μJ/cm^2.

1. Evaluation of the lifetimes

Figure 13 shows the PL decay curves and the time-integrated PL spectrum (inset) for a CdSe/MgS QD sample. The excitation power was 0.3 μJ/cm^2. In the PL spectrum, the emissions from the QD's, the WL, and the ZnSe buffer layer are clearly observed. The PL decays shown in the figure were measured at the energy positions designated by from *a* to *e* in the inset. The transitions detected near the maximum and on the low-energy side of the QD emission (*a* and *b*) decay monoexponentially, while those detected on the high-energy side (*c* and *d*) exhibit an additional faster component. Also at the WL emission (*e*), two decay components are resolved.

Again, lifetimes were evaluated using Eq. (1), and the results are shown in Fig. 14. In order to identify the origins

of these four transitions we note that there are three possible pathways in principle—that is, radiative recombination, nonradiative recombination, and relaxation toward a lower-energy level. Therefore, the PL lifetime can be written as $\tau_{PL}^{-1} = \tau_r^{-1} + \tau_{nr}^{-1} + \tau_{rl}^{-1}$, where τ_{rl} is the relaxation lifetime. In the followings, we discuss the physics behind the observed lifetimes.

2. Carrier dynamics in the QD's

We attribute the slow and fast transitions in the QD's to the radiative recombination involving the QD ground level and to the relaxation from a higher-energy excited level to the ground level, respectively. The reasons are described below.

a. Slow decay. In Sec. II, we calculated the spontaneous emission lifetime of 1*s* heavy-hole excitons. As can be seen in Fig. 3(c), the lifetime is basically longer for disks with a stronger lateral confinement. This is because a strong confinement in real space causes the spread of the wave vector of excitons in *k* space and reduces the number of excitons that can recombine radiatively. Therefore, the lifetime of QD's should be longer than that of QW's [typically ~300 ps in this study, as discussed with Fig. 8(a)], and, thus, the slow decay in the QD's was attributed to the spontaneous emission lifetime.

According to the theory that we adopted here, the spontaneous emission lifetime of quantum disks much smaller than the exciton resonance wavelength in materials is expressed by

$$\tau_r^{-1} = \frac{2e^2 n_r \omega_{ex}^2 \beta^2}{m_0 \varepsilon_0 c^3} \frac{(2M_b^2/3)F^2|\phi_{1s}(0)|^2}{m_0 \hbar \omega_{ex}}, \quad (4)$$

where n_r is the refractive index, ω_{ex} is the exciton resonance frequency, β is a parameter describing the exciton center-of-mass motion, m_0 is the electron mass, ε_0 is the static dielectric constant, *c* is the speed of light, M_b is the transition matrix element for bulk materials, *F* is the overlap integral between the electron and hole wave functions, and $\phi_{1s}(r)$ is the wave function for the exciton relative motion. Equation (4) tells us that the radiative lifetime within a PL spectrum
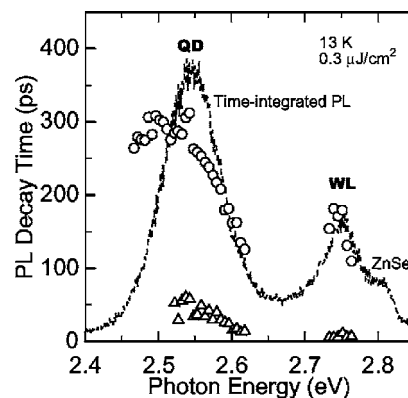

FIG. 14. PL decay times as a function of the emission energy. The open circles and triangles represent slow and fast PL decay, respectively, evaluated using Eq. (1).
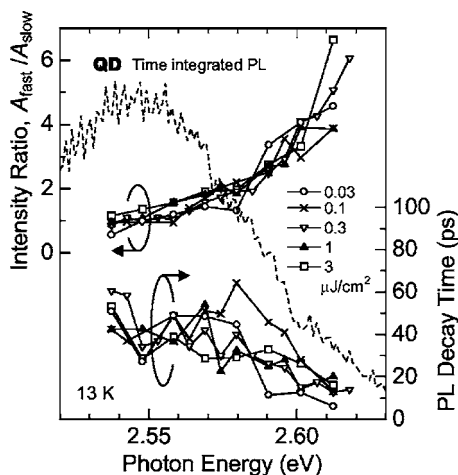
FIG. 15. Intensity ratio between the fast- and slow-decay components and fast-decay time in the energy range of the QD emission. The dependences on the excitation power are shown.

FIG. 16. cw PL spectra resonantly excited by the energies shown in the figure.

should be almost constant or rather longer for higher photon energy.[50] The experimental result shown in Fig. 14 exhibits a trend opposite to the theoretical expectation and indicates the presence of additional factors to be taken into account, though these have not been clarified yet. Very similar characteristics have been reported for InAs/GaAs[33,34] and CdSe/ZnSe QDs,[35] and so these can be introduced briefly. For example, Heitz *et al.*[33] pointed out the influence of nonradiative recombination, but nonradiative recombination is usually negligible at low temperatures. Lateral transfer of excitons between the QD's has also been proposed,[34,35] though the small density of QD's in the present sample (5 $\times 10^8$ cm^{-2} estimated by AFM) might prevent interdot transfer. Also, no lateral transfer was detected even at elevated temperatures (see Fig. 12). These models do not seem to account for the present results, and a further study will be necessary to identify the mechanism.

b. Fast decay. The faster-decay time decreases from 50 to 10 ps by increasing the detecting energy from 2.53 to 2.62 eV. Since the slow decay was attribute to the radiative decay, the remaining two factors—that is, nonradiative decay and intradot relaxation—are considered. Figure 15 compares the variations of the intensity ratio between the fast- and slow-decay components and of the fast-decay time due to the excitation power. The intensity ratio is independent of the excitation power, indicating that the observed fast transition is not a defect-related nonradiative process because the intensity of such a transition should depend on the excitation power due to the state-filling effect. Therefore, the carrier relaxation from an excited level to the ground level is the most probable origin of the fast decay. The contribution of higher levels is also supported by the experimental finding that the fast transition appears only on the high-energy side of the QD emission (see Fig. 13, for example). In the excitation power regime investigated in this study, emission from an excited level was not observed explicitly, indicating that its radiative lifetime is much longer than the relaxation time.
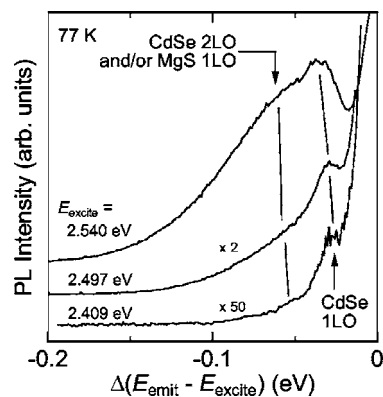
Figure 15 also gives an insight into the relaxation process from an excited level to the ground level. Since the fast decay time does not depend on the excitation power, the relaxation process does not involve carrier-carrier scattering. This is consistent with the results of resonantly excited cw-PL measurements shown in Fig. 16. In these spectra, resonances appear at the energy positions corresponding to CdSe 1LO (26 meV) and CdSe 2LO and/or MgS 1LO (55 meV), suggesting that LO phonon scattering is the primary intradot (intersublevel) relaxation process in the CdSe/MgS QD's under the present experimental conditions. Namely, photogenerated excitons relax from an excited level to the ground level with an assistance of the LO phonons and, subsequently, recombine radiatively.

The intradot relaxation time has extensively been studied for CdSe nanoparticles (surrounded by glass)[36–38] and In(Ga)As/GaAs self-assembled QD's.[33,39–41] The reported values vary widely from subpicosecond to a few hundreds picoseconds, and various mechanisms, such as carrier-carrier scattering, multiphonon emission, and biexciton formation, have been proposed.[33,36–41] The relative importance of these processes depends on, for example, the material system, the lattice temperature, the excitation power, and the QD dimensions. In CdSe nanoparticles, the intradot relaxation time of from 250 fs to 3 ps was reported and the mechanism behind it has been proposed to be Auger-type electron-hole scattering[36,37] and LA-phonon scattering and biexciton formation.[38] As reported in Refs. 40 and 41, the LO-phonon-related process is slower than other processes, and so the present assignment of the observed lifetime of 10–50 ps to the phonon process seems reasonable. A further support is given by Ref. 33, where a similar intradot relaxation lifetime of 28 ps has been reported for InAs/GaAs QD's and multi-LO-phonon scattering is proposed to be the dominant pathway for the carrier relaxation.

c. Temperature dependence. The temperature dependence of the QD PL decay measured with an excitation power of 3 μJ/cm^2 is summarized in Fig. 17. We begin by discussing the slow decay, which is the radiative decay at low temperatures. The lifetime is stable up to 50 K, as theoretically expected for the radiative recombination in QD's having the
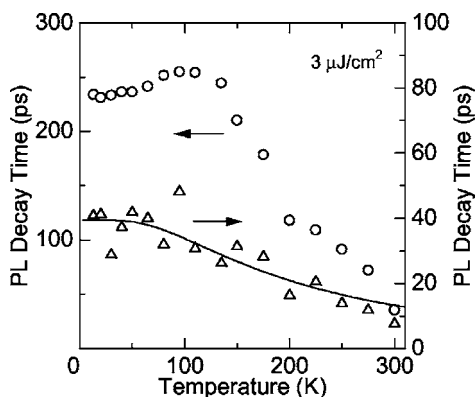
FIG. 17. Temperature dependence of the QD PL decay time. The open circles and triangles represent the slow and fast decay, respectively. The solid curve is the result of a fit. See the text for the detail.
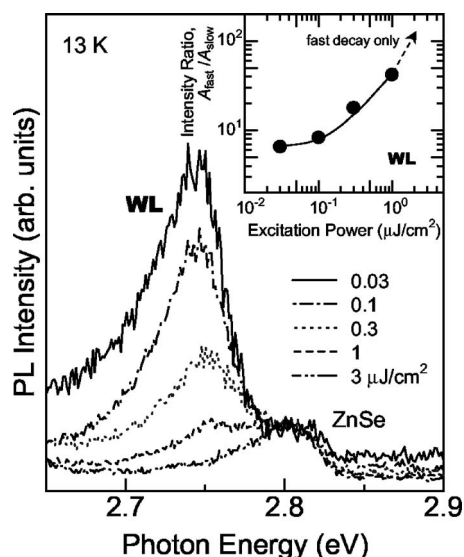

FIG. 18. Time-integrated PL spectra of WL (and ZnSe) under different excitation powers. The spectra were normalized with respect to the ZnSe emission. The inset is the intensity ratio between the fast and slow decays as a function of the excitation power.

density of states expressed by a δ function.[18] Then, it rises slightly up to 120 K, contrary to the theoretical expectation. However, such an increase in the radiative lifetime has been reported many times, particularly for InAs/GaAs self-assembled QD's, and is often attributed to the thermalization of excitons toward excited levels and/or thermally activated exciton transfer between QD's.[42–46] At least, the lateral exciton transfer can be ruled out in the present QD samples because no lateral transfer was detected even at elevated temperatures (Fig. 12). Rather, we have to consider the dimensionality of the QD's which are not perfect zero-dimensional QD's. As a consequence of a certain dimension, they should demonstrate properties intermediate between zero- and two-dimensional quantum structures.[47] Since the radiative lifetime of (two-dimensional) QW's is proportional to temperature, an increase in the radiative lifetime can occur in our QD's. Above 135 K, a drop of the lifetime occurs probably due to the thermal activation of nonradiative processes.

The faster decay, on the other hand, was attributed to the carrier relaxation via the interaction with LO phonons. Noting that LO phonons are emitted in this case, the relaxation time can be expressed by Eq. (3) with $A=1$ and a good fit was obtained by $E_{LO}=22.7$ meV, $m=1$, and $n=2$ as shown by the solid curve in Fig. 17, suggesting that the emission of two CdSe LO phonons is the main relaxation process from an excited level to the ground level. This result is consistent with resonantly excited PL shown in Fig. 16, where LO-phonon resonances are clearly seen. It is also interesting to compare the experimental results with the calculation shown in Fig. 3. The experimentally obtained radiative lifetime was $\sim$250 ps, and the emission peak energy was $\sim$2.5 eV. The thickness and radius of QD's that satisfy these quantities are estimated from Figs. 3(a) and 3(c) to be 1.5 nm and 5 nm, respectively. In such QD's, the energy separation between the first and second excited levels is determined by the lateral confinement and was calculated to be 42 meV. This agrees reasonably well with the total energy of two CdSe LO phonons (52 meV) and supports the model proposed above.

3. Carrier dynamics involving the WL

Comparing with the radiative lifetimes of ML-QW and QD's revealed above, we attribute the slower decay of 100–150 ps in the WL to the radiative decay. The reason why the radiative lifetime is the shortest for WL again relates to the dimensionality [cf. Eq. (4)]; QD's provide three-dimensional confinement and so does the ML-QW because of thickness fluctuations in both the growth and in-plane directions, while the WL possesses a certain thickness, the so-called critical thickness, and provides only one-dimensional confinement in the growth direction. The relatively narrow PL linewidth seen in Fig. 4 supports this assertion.

The origin of the fast decay of about 5 ps is discussed using Fig. 18. Under weak excitation the emission from the WL is visible, but its intensity is drastically weakened by more intense excitation. At the same time, the faster decay becomes dominant, as shown in the inset. These results indicate that the fast decay is neither radiative nor nonradiative decay because the radiative recombination would be in-
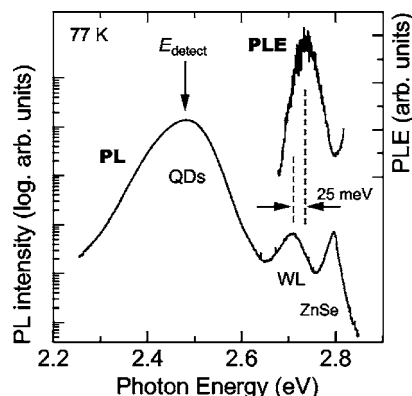

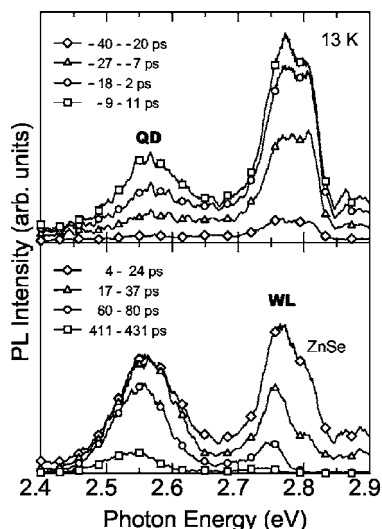FIG. 19. PL and PLE spectra of the QD sample.

FIG. 20. TRPL spectra of a CdSe/MgS QD.

creased by the stronger excitation and because the nonradiative component would be saturated with increasing the excitation power due to the state-filling effect. Therefore, we attribute this fast decay to the carrier relaxation from the WL to QD's. Since the emission disappears—that is, the relaxation is activated under strong excitation—it is inferred that the relaxation process occurs via carrier-carrier scattering.

The carrier relaxation from WL to QD is also demonstrated by PLE spectroscopy, in which PL was detected at the peak of the QD emission while the excitation energy was scanned in the energy range corresponding to the WL emission. Figure 19 shows the PL and PLE spectra. It is clear that the selective excitation of the WL strengthens the QD emission. A stokes shift of 25 meV detected between the WL emission and WL absorption (i.e., PLE peak) is due to a potential fluctuation in the WL giving a PL linewidth of about 40 meV, in reasonable agreement with the Stokes shift.

For InAs/GaAs, the Auger scattering is proposed as the dominant process for carrier relaxation from WL to QD's,[48] and the reported lifetime is quite short ($<$5 ps),[33] consistent with the present study.

4. Summary of the carrier dynamics

The carrier dynamics discussed above can well be seen in the TRPL spectra shown in Fig. 20. PL from WL (and ZnSe) is first developed and reaches the maximum at −9−11 ps as shown in the upper panel. With a slight delay, the QD PL gets stronger and reaches a maximum at 4−37 ps. The difference of the time at which WL-PL and QD-PL reaches a maximum is roughly 20 ps. This behavior can be interpreted
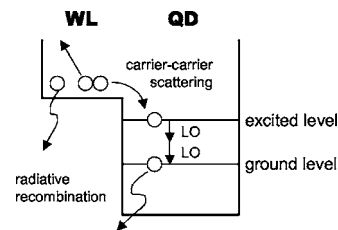

FIG. 21. Schematic illustration of the carrier dynamics in the present CdSe/MgS QD's.

as follows. At first, carriers are directly generated in the WL by the excitation at 400 nm (=3.10 eV), which is between the WL energy gap and the MgS energy gap. Some of them recombine radiatively in WL, while some transfer into QD's, relax to the ground level, and emit radiatively. It presumably takes about 20 ps for carriers to travel from the WL to the ground level in the QD's. From the PL decay, on the other hand, we estimated the carrier transfer time from WL to QD to be ~5 ps and the intradot relaxation time to be 10−50 ps. Totally, the QD emission should follow the WL emission 15−55 ps later, which is in reasonable agreement with the delay of ~20 ps observed in Fig. 20. After reaching the maximum, the WL emission disappears more quickly, reflecting a radiative lifetime shorter than that of QD's. The QD emission quenches from the high-energy side due to the shorter lifetime on this side (see Fig. 14). Figure 21 schematically summarizes the proposed carrier dynamics in the present CdSe/MgS sample.

VII. SUMMARY

The optical properties of CdSe/MgS ML-QW's and QD's were investigated. The growth development from ML-QW to SK-QD's is clearly shown by the cw-PL measurements. For the QW's, carrier localization in potential fluctuations and scattering by phonons play an important role in determining the optical properties. For SK-QD's, it was found that some of the carriers photogenerated in the WL emit radiatively and some are captured by QD's via carrier-carrier scattering on a time scale of ~5 ps. Within the next 10−50 ps, the carriers relax to the ground level via a carrier–LO-phonon scattering. Finally, the carriers recombine radiatively with a recombination lifetime of 100−300 ps, depending on the emission energy.

*Electric mail: funato@kuee.kyoto-u.ac.jp

†Present address: Nichia Corporation, Tokushima 774-8601, Japan.

[1] D. Bimberg, M. Grundmann, and N. N. Ledevtsov, *Quantum Dot Heterostructures* (Wiley, New York, 1999).

[2] C. S. Kim, M. Kim, S. Lee, J. Kossut, J. K. Furdyna, and M. Dobrolowska, J. Cryst. Growth **214/215**, 395 (2000).

[3] Y. Oka, J. Shen, K. Tabayashi, N. Takahashi, H. Mitsu, I. Souma, and R. Pittini, J. Lumin. **83/84**, 83 (1999).

[4] X. Tang, B. Urbaszek, T. C. M. Graham, R. J. Warburton, K. A. Prior, and B. C. Cavenett, J. Cryst. Growth **251**, 586 (2003).

[5] S. Xin, P. Wang, A. Yin, C. Yin, M. Dobrowolska, J. Merz, and J. Furdyna, Appl. Phys. Lett. **69**, 3884 (1996).

[6] I. Suemune, K. Uesugi, H. Suzuki, H. Nashiki, and M. Arita, Phys. Status Solidi B **202**, 845 (1997).

[7] H. C. Ko, D. C. Park, Y. Kawakami, S. Fujita, and S. Fujita, Appl. Phys. Lett. **70**, 3278 (1997).

[8] M. Strassburg *et al.*, Appl. Phys. Lett. **76**, 685 (2000).

[9] K. Sebald, P. Michler, T. Passow, D. Hommel, G. Bacher, and A. Forchel, Appl. Phys. Lett. **81**, 2920 (2002).

[10] Z. Zhu, H. Yoshihara, K. Takebayashi, and T. Yao, Appl. Phys. Lett. **63**, 1678 (1993).

[11] C. Bradford, C. B. O'Donnell, B. Urbaszek, C. Morhain, A. Balocchi, K. A. Prior, and B. C. Cavenett, Phys. Rev. B **64**, 195309 (2001).

[12] M. Funato, A. Balocchi, C. Bradford, K. A. Prior, and B. C. Cavenett, Appl. Phys. Lett. **80**, 443 (2002).

[13] D. Schikora, S. Schwedhelm, D. J. As, K. Lischko, D. Litvinov, A. Rosenauer, D. Gerthsen, M. Strassburg, A. Hoffmann, and D. Bimberg, Appl. Phys. Lett. **76**, 418 (2000).

[14] V. S. Sorokin, S. V. Sorokin, V. A. Kaygorodov, and S. V. Ivanov, J. Cryst. Growth **214/215**, 130 (2000).

[15] W. A. Harrison, J. Vac. Sci. Technol. **14**, 1016 (1977).

[16] P. Peyla, R. Romestain, Y. Merle d'Aubigné, G. Fishman, A. Wasiela, and H. Mariette, Phys. Rev. B **52**, 12026 (1995).

[17] D. Gammon, E. S. Snow, B. V. Shanabrook, D. S. Katzer, and D. Park, Phys. Rev. Lett. **76**, 3005 (1996).

[18] M. Sugawara, Phys. Rev. B **51**, 10743 (1995).

[19] R. H. Yan, S. W. Corzine, L. A. Coldren, and I. Suemune, IEEE J. Quantum Electron. **QE-26**, 213 (1990).

[20] W. Shan, J. J. Song, H. Luo, and J. K. Furdyna, Phys. Rev. B **50**, 8012 (1994).

[21] T.-Y. Chung, J. H. Oh, S.-G. Lee, J.-W. Jeong, and K. J. Chang, Semicond. Sci. Technol. **12**, 701 (1997).

[22] H. J. Lozykowski and V. K. Shastri, J. Appl. Phys. **69**, 3235 (1991).

[23] Y. h. Wu, IEEE J. Quantum Electron. **30**, 1562 (1994).

[24] Y. Morinaga, H. Okuyama, and K. Akimoto, Jpn. J. Appl. Phys., Part 2 **31**, L340 (1993).

[25] N. Samarth, H. Luo, J. K. Furdyna, S. B. Qadri, Y. R. Lee, A. K. Ramdas, and N. Otsuka, Appl. Phys. Lett. **54**, 2680 (1989).

[26] M. Rabe, M. Lowisch, and F. Henneberger, J. Cryst. Growth **185**, 248 (1998).

[27] S. Fujita, Y. h. Wu, Y. Kawakami, and S. Fujita, J. Appl. Phys. **72**, 5233 (1992).

[28] C. Gourdon and P. Lavallard, Phys. Status Solidi B **153**, 641 (1989).

[29] L. Aigouy, V. Mathet, F. Liaci, B. Gil, O. Briot, N. Briot, T.

Cloitre, M. Averous, and R. L. Aulombard, Phys. Rev. B **53**, 4708 (1996).

[30] T. Inoshita and H. Sakaki, Phys. Rev. B **46**, 7260 (1992).

[31] J. K. Furdyna, S. Lee, A.-L. Barabási, and J. L. Merz, *II-VI Semiconductor Materials and their Applications* (Talor & Francis, London, 2002), Chap. 9.

[32] S. Ninomiya and S. Adachi, J. Appl. Phys. **78**, 4681 (1995).

[33] R. Heitz, M. Veit, N. N. Ledentsov, A. Hoffmann, D. Bimberg, V. M. Ustinov, P. S. Kop'ev, and Z. I. Alferov, Phys. Rev. B **56**, 10435 (1997).

[34] A. Tackeuchi, Y. Nakata, S. Muto, Y. Sugiyama, T. Usuki, Y. Nishiwaka, N. Yokoyama, and O. Wada, Jpn. J. Appl. Phys., Part 2 **34**, L1439 (1995).

[35] M. Strassburg, M. Dworzak, H. Born, R. Heitz, A. Hoffmann, M. Bartels, K. Lischka, D. Schikora, and J. Christen, Appl. Phys. Lett. **80**, 473 (2002).

[36] P. Guyot-Sionnest, M. Shim, C. Matranga, and M. Hines, Phys. Rev. B **60**, R2181 (1999).

[37] V. I. Klimov, A. A. Mikhailovsky, D. W. McBranch, C. A. Leatherdale, and M. G. Bawendi, Phys. Rev. B **61**, R13349 (2000).

[38] U. Woggon, H. Giessen, F. Gindele, O. Wind, B. Fluegel, and N. Peyghambarian, Phys. Rev. B **54**, 17681 (1996).

[39] S. Raymond, S. Fafard, P. J. Poole, A. Wojs, P. Hawrylak, S. Charbonneau, D. Leonard, R. Leon, P. M. Petroff, and J. L. Merz, Phys. Rev. B **54**, 11548 (1996).

[40] B. Ohnesorge, M. Albrecht, J. Oshinowo, A. Forchel, and Y. Arakawa, Phys. Rev. B **54**, 11532 (1996).

[41] M. D. Giorgi, C. Lingk, G. von Piessen, J. Feldmann, S. D. Rinaldis, A. Passaseo, M. D. Vittorio, R. Cingolani, and M. Lomascolo, Appl. Phys. Lett. **79**, 3968 (2001).

[42] H. Yu, S. Lycett, C. Roberts, and R. Murray, Appl. Phys. Lett. **69**, 4087 (1996).

[43] W. Yang, R. R. Lowe-Webb, H. Lee, and P. C. Sercel, Phys. Rev. B **56**, 13314 (1997).

[44] L. Zhang, T. F. Boggess, D. G. Deppe, D. L. Huffaker, O. B. Shchekin, and C. Cao, Appl. Phys. Lett. **76**, 1222 (2000).

[45] T. F. Boggess, L. Zhang, D. G. Deppe, D. L. Huffaker, and C. Cao, Appl. Phys. Lett. **78**, 276 (2001).

[46] M. Pailard, X. Marie, E. Vanelle, T. Amand, V. K. Kalevich, A. R. Kovsh, A. E. Zhukov, and V. M. Ustinov, Appl. Phys. Lett. **76**, 76 (2000).

[47] H. Gotoh, H. Ando, and T. Takagahara, J. Appl. Phys. **81**, 1785 (1997).

[48] S. Raymond, K. Hinzer, S. Fafard, and J. L. Merz, Phys. Rev. B **61**, R16331 (2000).

[49] The rate for a defect capturing carriers—that is, the nonradiative recombination rate τ_{nr}^{-1}—is expressed as $\tau_{nr}^{-1} = v_{th} N_t \sigma$, where v_{th} is the thermal velocity, N_t is the density, and σ is the capture cross section. Since $v_{th} \propto T^{1/2}$, we get a relation $\tau_{nr} \propto T^{-1/2}$.

[50] In Eq. (4), variables with respect to the photon energy are ω_{ex} and β. The variation of ω_{ex} is negligibly small within the PL emission peaking at 2.55 eV with a width of ~ 100 meV, while β becomes rather smaller for higher photon energy. (This is understandable by considering that small β means a small dot, in which excitons are highly confined.) As a consequence, the radiative lifetime becomes longer for higher energy.